Experimental Adsorption Isotherm of Methane onto Activated Carbon at Sub- and Supercritical Temperatures

Kazi Afzalur Rahman,[†] Wai Soong Loh,[†] Hideharu Yanagi,[†] Anutosh Chakraborty,[‡] Bidyut Baran Saha,[§] Won Gee Chun,[||] and Kim Choon Ng*[,†]

Department of Mechanical Engineering, National University of Singapore, 9 Engineering Drive 1, Singapore 117576, School of Mechanical and Aerospace Engineering, Nanyang Technological University, 50 Nanyang Avenue, Singapore 639798, Department of Mechanical Engineering, Kyushu University, 744 Motooka, Nishi-ku, Fukuoka 819-0395, Japan, and Department of Nuclear and Energy Engineering, Cheju National University, 66 Jejudaehakno, Jejusi, South Korea

This paper presents the experimentally measured adsorption isotherm data for methane onto the pitch-based activated carbon type Maxsorb III for temperatures ranging from (120 to 220) K and pressures up to 1.4 MPa. These data are useful to study adsorbed natural gas (ANG) storage systems when the low temperature natural gas regasified from the liquid phase is considered to charge in the storage chamber. Adsorption parameters were evaluated from the isotherm data using the Tóth and Dubinin−Astakhov models. The isosteric heat of adsorption, which is concentration- and temperature-dependent, is extracted from the data. The Henry's law coefficients for the methane/Maxsorb III pairs are evaluated at various temperatures.

Introduction

Natural gas (NG) has long been considered as an alternative fuel in transportation technology, as it provides better combustion and minimizes exhaust pollutants. It is mostly composed of methane, CH_4, and has the highest heating value per unit mass (50.1 $MJ \cdot kg^{-1}$, lower heating value)[1] of the hydrocarbon fuels (e.g., butane, diesel fuel, gasoline, etc.). Moreover, its lower price and copious availability make it more attractive as vehicular fuel. More than half of the world's conventional natural gas is found in the Persian Gulf and Russia. The natural gas is generally stored and supplied either using compressed natural gas (CNG) at high pressures up to 300 bar or by liquefied natural gas (LNG) at cryogenic temperature, that is, −160 °C at ambient pressure. Both methods are costly for their distribution and reticulation, especially LNG which requires extensive cooling energy to maintain the low temperature. However, LNG is 600 times denser than the gaseous phase, and it is preferred compared to CNG in storage and distribution to remote places where pipeline transportation may be unavailable. Thus, LNG makes natural gas a fungible commodity like oil and can be shipped to LNG terminals located in different parts of the world.

The LNG can then be converted into the gaseous phase using heat from seawater and distributed through pipelines from the terminal to the utilities that consume NG as the energy source. Adsorbed natural gas (ANG) is one of the energy storage systems and has recently attracted much attention as an alternative to CNG for energy storage and transportation purposes. The ANG system can be designed to a higher energy density yet operates at a lower pressure than the CNG method.[1−18] In ANG storage, the gas molecules are captured into the micro- and mesopores of the adsorbent at a liquid-like density in the adsorbed phase, providing a higher storage density than compression alone. The ANG vessel is charged with a suitable amount of NG so that the storage equilibrium pressure is controlled to a desired pressure of 4 MPa or less.

Although extensive studies have been investigated on aspects of adsorption characteristics of methane by activated carbons at assorted pressures and temperatures,[11−17] the adsorption parameters of methane at subcritical temperatures in AC are scarcely reported in the literature. Hence, the objective of the present study is to provide such data of methane on AC at conditions below the critical point, typically the charging of cold NG vapor at (−150 to −70) °C to the adsorbent in an ANG storage vessel, a process that is similar to the regasification of LNG.

To date, the most promising adsorbents for ANG storage are the highly microporous activated carbons[11−24] with relatively high packing densities[16,17] and higher specific surface areas.[25] In this study, the adsorption isotherms of methane on pitch-based activated carbon type Maxsorb III are measured using a constant-volume−variable-pressure (CVVP) apparatus. The temperatures are maintained at subcryogenic ranges from (120 to 220) K using a purpose-built cryostat and pressures up to 1.4 MPa. Adsorption parameters are evaluated from the isotherm data using the Tóth and Dubinin−Astakhov (DA) models. The heat of adsorption (H_{ads}) and the Henry's constant (K_H) are also calculated from the isotherm data.

Materials and Experiments

Activated Carbon and the Methane. An ultrapure methane sample at a purity grade of 99.9995 % was used for the present experiment. The Maxsorb III, which was in powder form and highly microporous, was used as the solid adsorbent. This sample was developed from various kinds of petroleum coke, and the production procedures have been reported by Otowa et al.[26] Table 1 tabulates the properties of Maxsorb III, such as the Brunauer−Emmett−Teller (BET) surface area, pore size, pore volume, porosity, and the skeletal density. These thermo-

* Corresponding author. Professor Kim Choon Ng, Department of Mechanical Engineering, National University of Singapore, 9 Engineering Drive 1, Singapore 117576. Phone: +65 65162214. E-mail: mpengkc@nus.edu.sg.
[†] National University of Singapore.
[‡] Nanyang Technological University.
[§] Kyushu University.
[||] Cheju National University.

10.1021/je1005328
Published on Web 09/20/2010

Table 1. Thermophysical Properties of Maxsorb III

BET surface area [$m^2 \cdot kg^{-1}$]	$3.14 \cdot 10^6$
total pore volume [$m^3 \cdot kg^{-1}$]	$20.1 \cdot 10^{-4}$
micro pore volume [$m^3 \cdot kg^{-1}$]	$1.79 \cdot 10^{-4}$
average pore diameter [Å]	20.08
skeleton density [$kg \cdot m^{-3}$]	2200
apparent density [$kg \cdot m^{-3}$]	156
particle porosity	0.81

physical properties were measured using an Autosorb (Quantachrome gas sorption instrument) machine: The surface area was calculated by the BET method from the N_2 adsorption isotherm data, which has been performed at 77.3 K. The pore size distribution (PSD) of Maxsorb III has been obtained by the nonlocal density functional theory (NLDFT) method. The skeletal density of the sample was measured by an automated Micromeritics AccuPyc 1330 pycnometer at room temperature. Figure 1 shows a scanning electron microscope (SEM) photograph of Maxsorb III, where the surface structure is observed to be flake-like layers with porous volumes entrenched between the layers.

Experimental Apparatus. The experimental apparatus is described in two sections: (i) the volumetric apparatus to measure the uptake for an adsorbate−adsorbent pair at different isothermal conditions and (ii) the cryostat to maintain the adsorption chamber at constant cryogenic temperatures.

Volumetric Apparatus. A schematic of the volumetric adsorption apparatus is shown in Figure 2a. It consists of a charging chamber and an adsorption chamber which is placed inside a cryostat. The charging chamber is made of stainless steel (SS 304) with an internal volume of (2215 ± 5) cm^3 including the connections of the charging side. A pressure transducer and a resistance temperature device (RTD) type temperature sensor are connected with suitable fittings to monitor the pressure and temperature of the charging chamber which is immersed in a constant-temperature water bath. The adsorption chamber is made of Ni−Cr plated copper with internal volume of (64 ± 1) cm^3 and wrapped with a 1/4″ copper coil through which liquid N_2 will flow. A manganese-wire heater (90 W capacity) is also installed in the cryostat to maintain a variety of cryo-temperatures. The Maxsorb III sample is weighed by a moisture analyzer with an uncertainty of ± 0.1 mg, and an amount of 9.9754 g is packed into the adsorption chamber. The adsorption chamber hangs inside a stainless steel vacuum chamber from an annular protrusion of the vacuum flange through 1/8″ stainless steel tubing. A 0.5 μm stainless steel sintered filter is also fitted to the adsorption chamber to stop the migration of adsorbent particles during evacuation. A set of Swagelok fittings (valves, T's, and reducers) and the 1/4″ nominal stainless steel capillary tubing is used after the filter to connect the adsorption chamber to the charging side. The total internal volume of the capillary tubing for adsorption side is estimated to be 3.7 cm^3. A class-A RTD temperature probe is inserted at the bottom of the adsorption chamber to measure the adsorbent temperature, and a pressure transducer is connected to monitor the chamber pressure.

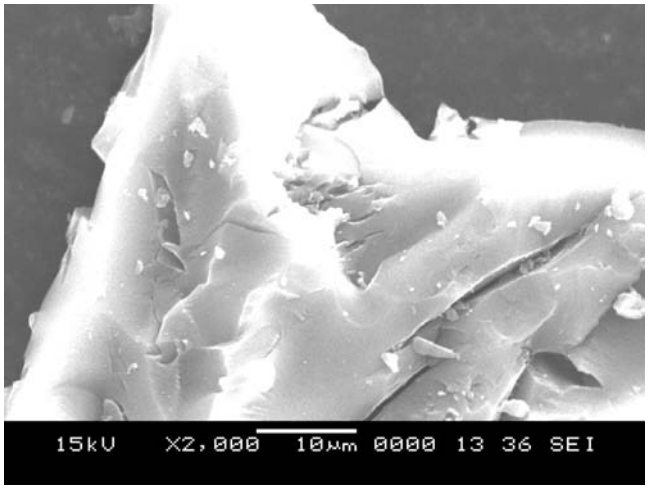

Figure 1. SEM photograph of the Maxsorb III sample (2000 magnification).

Cryostat. Figure 2b shows the schematic of the cryostat and the arrangement of the adsorption chamber. The vacuum chamber, which is the main building block of the cryostat, is evacuated by a diffusion-type vacuum pump to build the vacuum insulation for the adsorption chamber. The appropriate vacuum fittings are used to maintain a vacuum level of 0.013 Pa. The inlet/outlet tubes for liquid N_2 flow are passed through the 50 mm long annular protrusions of the KF-16 vacuum flange and are welded at the outer end of the annulus. A gap is kept between the annular protrusion and the tube to prevent the conduction of heat through the vacuum flange. However, a small amount of heat could be radiated due to the high temperature gradient between ambience and the adsorption chamber. Hence, a continuous flow of liquid N_2 is required to maintain cryo-temperatures. The liquid N_2 is supplied from a 50 L Dewar tank through a manual discharge device, and compressed N_2 gas is used to ensure a constant liquid N_2 flow rate. A hermetic feed-through is also connected to the vacuum flange to transmit the electrical signals and supply current to the heater. The adjustable direct current (DC) power is supplied to the heater to achieve a constant temperature, while the liquid N_2 is flowing at a constant rate.

Instrumentation. The pressure readings of methane were measured using a (0 to 5) MPa range Kyowa pressure transducer (PGS-50KA) with an uncertainty of ± 0.1 % of full scale in measurement. The temperatures were recorded using Pt 100 Ω RTDs with an estimated uncertainty of ± 0.1 K for the charging side and ± 0.2 K for the adsorption side ranging from (73 to 473) K. An Agilent 34970A data acquisition system connected to the computer was used to monitor the temperature and pressure readings. A constant-temperature water bath (Haake F8-C35) gives a stability of ± 0.01 K and was used to maintain the charging temperature. The cryostat was monitored to maintain a preselected temperature of (110 to 230) K with a stability of ± 1 K. The maximum overall uncertainty associated with the instrumentation is within 5 %, which is typical using the volumetric method.[15]

Procedures. Prior to the experiment, the adsorption chamber was evacuated for 24 h to a vacuum level of 10^{-3} mbar, and a regeneration temperature of about (140 to 150) °C was maintained to enhance the removal of residue gas in the adsorbents. Pure helium gas was purged into the system during regeneration to improve the evacuation of the cylinders. After evacuation, the cryostat was turned on with the vacuum chamber kept in vacuum, and the liquid N_2 flowed through the copper coil around the adsorption chamber. The manual discharge device was operated to charge the liquid N_2 out from the Dewar tank, and a constant flow rate was achieved by maintaining the tank pressure. At the same time, the heater was adjusted accordingly, using the DC power supply to obtain an isothermal condition for a respective temperature range from (110 to 230) K. The nitrogen vapor that leaves the cryostat was purged into a fume hood. When the temperature was stabilized, methane vapor was released into the adsorption side from the charging

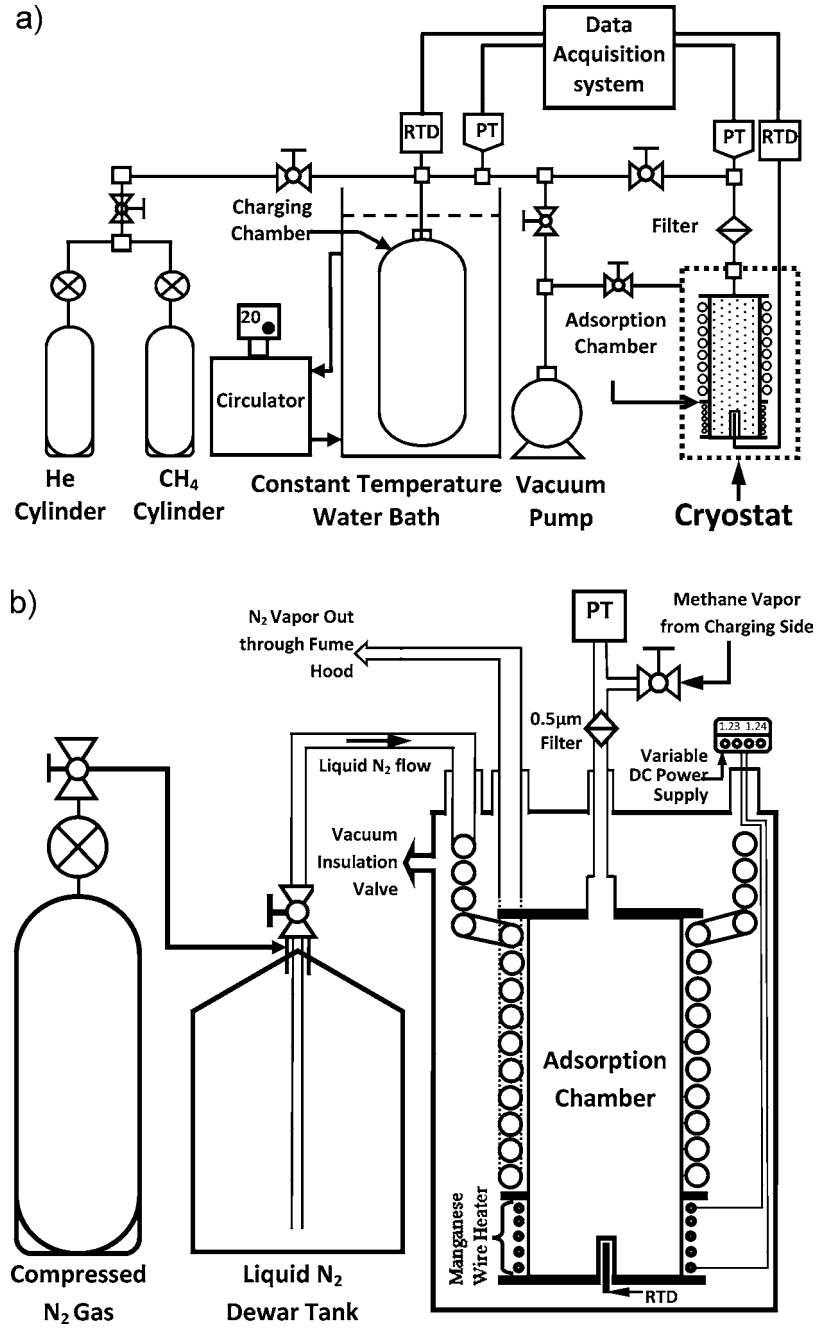

Figure 2. (a) Schematic diagram of the volumetric apparatus. (b) Schematic diagram of the cryostat.

chamber which had been filled with methane vapor at a definite pressure and immersed in the constant-temperature water bath. Figure 3 provides the typical pressure and temperature profiles of the adsorption chamber after the methane vapor releases. The temperature rise was due to the evolution of heat during the adsorption process, and a rapid drop in the adsorption side pressure (indicated by dotted circular mark) was due to the shutting off of the valve connecting the charging chamber. Both the pressure and the temperature stabilized after the adsorption chamber reached the equilibrium state, and the readings were recorded every 10 s. The adsorbed mass of methane was calculated from the amount of vapor transferred to the adsorption chamber and the leftover amount at the equilibrium state. Similarly, the adsorption chamber was charged to the next higher pressure with the same cryostat condition for the subsequent data point. Measurements were made up to 1.4 MPa, and the same procedures were repeated with different isotherms. At-

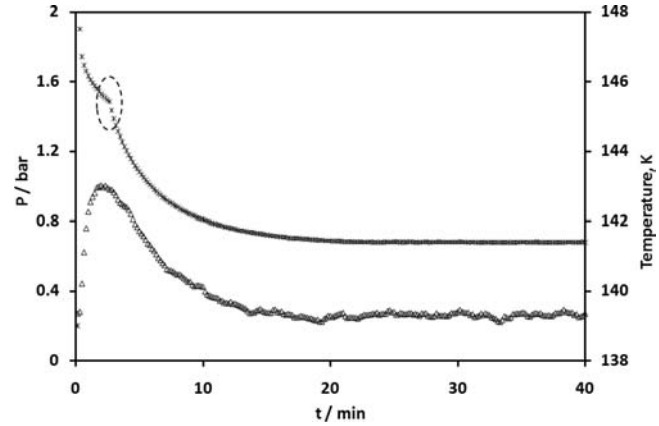

Figure 3. Typical pressure and temperature profiles during adsorption: ∗, pressure (left ordinate); △, temperature (right ordinate).

tention was given so that both the chamber pressures always remained below the saturation pressure to avoid condensation of methane vapor, especially in the adsorption chamber. To check the accuracy and reproducibility of the data points, we carried out several runs under identical conditions and obtained good reproducibility in all cases with deviations of the amount adsorbed smaller than 5 %.

Theoretical Analysis

The pressure (P) and temperature (T) readings of both the adsorption and the charging chamber were the raw data used to calculate the adsorption uptake (C) of the Maxsorb III/methane pair. The arithmetically averaged pressure (P_{avg}) and temperature (T_{avg}) at equilibrium state were used to measure the mass of methane from the density of the vapor and the chamber volumes. The density data for methane used in this paper were evaluated using the generalized equation of state proposed by Setzmann and Wagner.[27] At equilibrium, the methane transferred to the adsorption chamber (m_{ads_chm}) was partly adsorbed in the micro- and mesopores of the adsorbent, and the leftover vapor occupied the void volume (V_{void}). Thus, the adsorbed mass ($m_{adsorbed}$) was calculated from the following equations

$$m_{adsorbed}(P_{avg}, T_{avg}) = m_{ads\_chm} - \rho_{void}(P_{avg}, T_{avg})V_{void} \quad (1)$$

$$V_{void} = V_{ads\_chm} - \frac{m_{ac}}{\rho_{solid}}m_{ac} - \upsilon_{\mu}m_{ac} \quad (2)$$

where ρ_{void} is the density of nonadsorbed methane vapor as a function of pressure (P_{avg}) and temperature (T_{avg}) of the adsorption chamber, V_{ads_chm} is the adsorption chamber volume, m_{ac} is the mass of activated carbon sample in the adsorption chamber, ρ_{solid} is the solid density of activated carbon, and υ_{μ} is the microporous volume of activated carbon. Hence, the amount of methane uptake is calculated as $C(P_{avg},T_{avg}) = m_{adsorbed}/m_{ac}$. The experimentally measured uptake data at different isothermal conditions ($T_{isotherm}$) for adsorption of methane on Maxsorb III are furnished in Table 2.

The Tóth and the DA models have been used to correlate the experimental equilibrium uptakes. The Tóth model is used for heterogeneous adsorbents such as activated carbon because of its correct behavior at both low and high pressure,[28] which is expressed as

$$\frac{C}{C_0} = \frac{k_0 \exp(H_{ads}/RT)P}{\{1 + (k_0 \exp(H_{ads}/RT)P)^t\}^{1/t}} \quad (3)$$

where C_0 is the saturated amount adsorbed in kg·kg^{-1}, P is the equilibrium pressure, k_0 is the equilibrium constant, H_{ads} is the isosteric heat of adsorption, t is the parameter that indicates the heterogeneity of the adsorbent, and R is the gas constant.

The DA model for adsorption of vapors and gases onto nonhomogeneous carbonaceous solids[28] could account for surface heterogeneity and is expressed as

$$\frac{W}{W_0} = \exp\left[-\left\{\frac{RT}{E}\ln\left(\frac{P_s}{P}\right)\right\}^n\right] \quad (4)$$

Table 2. Experimental Uptake Data for Adsorption of Methane on Maxsorb III

T / K	P / kPa	C / kg·kg^{-1}	T / K	P / kPa	C / kg·kg^{-1}
$T_{isotherm}$ = 219.7 K			$T_{isotherm}$ = 199.8 K		
219.49	38.52	0.072	199.28	23.34	0.091
219.62	107.88	0.127	200.27	91.74	0.171
219.77	214.95	0.176	199.69	171.37	0.215
218.73	309.11	0.208	199.68	327.56	0.262
219.75	435.20	0.234	199.43	481.43	0.294
219.90	567.56	0.256	199.48	619.49	0.317
220.12	712.60	0.278	199.63	748.17	0.334
219.58	841.84	0.295	200.86	863.94	0.349
219.88	1065.09	0.319	199.49	1028.91	0.374
220.00	1256.73	0.337	199.99	1201.99	0.392
$T_{isotherm}$ = 179.0 K			$T_{isotherm}$ = 160.0 K		
179.32	13.00	0.114	160.86	41.85	0.270
178.99	72.64	0.226	159.80	177.86	0.401
178.76	173.03	0.287	160.59	231.10	0.432
179.08	287.61	0.327	159.65	321.56	0.479
178.74	406.32	0.355	160.06	360.68	0.508
179.60	515.32	0.376	159.64	448.57	0.525
179.69	639.03	0.403	159.25	564.63	0.566
179.09	717.87	0.424	159.81	730.60	0.599
178.40	792.44	0.443	160.14	856.76	0.633
179.19	948.99	0.467	159.96	994.14	0.646
179.61	1119.18	0.491			
$T_{isotherm}$ = 139.6 K			$T_{isotherm}$ = 120.2 K		
139.33	20.03	0.326	121.50	9.11	0.434
139.29	68.06	0.436	119.91	19.47	0.582
140.68	89.87	0.477	119.53	24.63	0.665
139.28	112.31	0.516	120.12	71.27	0.771
139.09	162.66	0.585			
140.57	168.30	0.599			
139.21	252.80	0.645			
140.08	303.85	0.708			
139.15	334.70	0.728			

where W is the amount of uptake in cm^3·g^{-1}, W_0 is the limiting uptake of adsorption space of the adsorbent in cm^3·g^{-1}, E is the characteristic energy of the adsorption system, and n is the structural heterogeneity parameter.

Ozawa et al.[29] have proposed a volume correction to the DA model considering the thermal expansion of the adsorbed phase. The specific volume of the adsorbed phase (υ_a) is estimated using the following equation for a wide range of temperatures in sequence with that used for high pressure gases.[29]

$$\upsilon_a = \upsilon_b \exp[\alpha[T - T_b]] \quad (5)$$

where υ_b is the specific volume of the liquid at the boiling point, T_b, and α is the thermal expansion coefficient of the adsorbed phase which can be expressed as follows from its definition.[13]

$$\alpha = \frac{1}{\upsilon_a}\left(\frac{\partial \upsilon_a}{\partial T}\right)_P \approx \frac{1}{T} \quad (6)$$

If the adsorbed phase volume is not taken into consideration, the DA model can also be reduced to the following equation.

$$\frac{C}{C_0} = \exp\left[-\left\{\frac{RT}{E}\ln\left(\frac{P_s}{P}\right)\right\}^n\right] \quad (7)$$

When the methane vapor is in a state above the critical temperature, the pseudovapor pressure, P_s, at a given temper-

ature is calculated by Dubinin's method[30] that has been used for methane in earlier studies.[13,15,31]

$$P_S = \left(\frac{T}{T_c}\right)^2 P_c \quad (T > T_c) \tag{8}$$

where P_c and T_c are the critical pressure and the critical temperature of methane, respectively.

Results and Discussion

Adsorption Isotherms. Experimentally measured uptake data at different isothermal conditions ($T_{isotherm}$) for the adsorption of methane on Maxsorb III are shown in Figure 4. The isotherm data have been measured for temperatures ranging from (120 to 220) K and pressures up to 1.4 MPa and regressed using the Tóth model with an average regression error of 6 %. The solid lines in Figure 4 represent the isotherms calculated from the Tóth model using the regressed adsorption parameters (C_0, k_0, H_{ads}, and t) that are listed in Table 3. As the Maxsorb III sample is highly microporous and heterogeneous in surface structure, the Tóth model provides a good representation due to the accountability of the heterogeneity parameter (t). The smaller value of the heterogeneity parameter (t) also indicates that the adsorbent surface is highly microporous and heterogeneous. Furthermore, the broken (dotted) line is predicted from the Tóth model using these regressed parameters for temperature at 298.15 K. The data points (cross symbols) for 298.15 K, reproduced from the author's experimental data for the same adsorbent (Maxsorb III),[32] closely agree with the current predictions. Therefore, this observation confirms that the uptake at higher temperature can be extrapolated using this model. However, it is obvious that the model will give a more accurate prediction when it is regressed for the whole range of isotherm data.

The DA model is employed to fit the uptake data as shown in Figure 5. The solid lines represent the adsorption isotherms

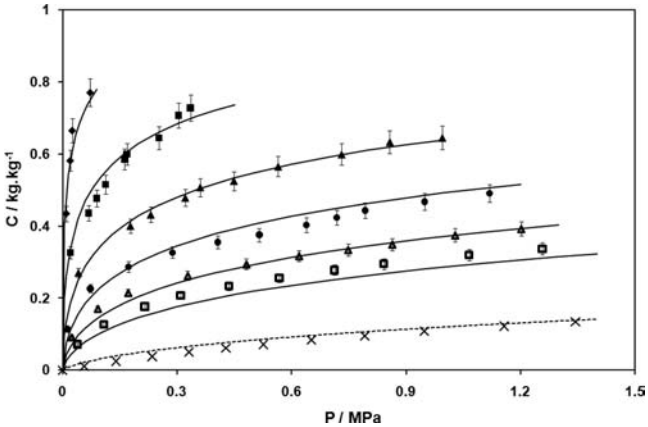

Figure 4. Adsorption isotherms of methane on Maxsorb III with error bars of 5 %: ♦, $T_{isotherm}$ = 120.2 K; ■, $T_{isotherm}$ = 139.6 K; ▲, $T_{isotherm}$ = 160.0 K; ●, $T_{isotherm}$ = 179.0 K; △, $T_{isotherm}$ = 199.8 K; □, $T_{isotherm}$ = 219.7 K. Solid lines are from the Tóth model. ×, uptake at 298.15 K from Loh et al.[32] The broken (dotted) line is from Tóth model at 298.15 K.

Table 3. Adsorption Parameters (C_0, k_0, H_{ads}, and t) for the Tóth Model

C_0 (kg·kg^{-1})	1.503
H_{ads} (kJ·kg^{-1})	867.68
k_0·10^3 (MPa^{-1})	3.65
t	0.274
average error of regression (%)	5.55

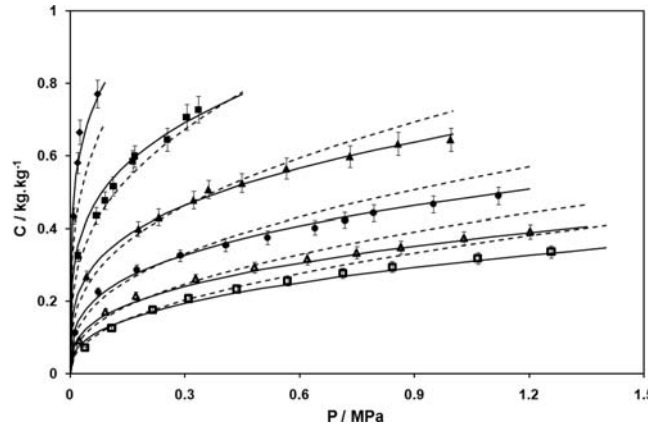

Figure 5. Adsorption isotherms of methane on Maxsorb III with error bars of 5 %: ♦, $T_{isotherm}$ = 120.2 K; ■, $T_{isotherm}$ = 139.6 K; ▲, $T_{isotherm}$ = 160.0 K; ●, $T_{isotherm}$ = 179.0 K; △, $T_{isotherm}$ = 199.8 K; □, $T_{isotherm}$ = 219.7 K. Solid lines are from the DA model with the adsorbed phase volume correction and the broken lines without considering the adsorbed phase volume.

Table 4. Adsorption Parameters (W_0/C_0, E, and n) for the DA Model

parameters	with the adsorbed phase volume correction	with no consideration of the adsorbed phase volume
W_0/cm^3·g^{-1} or C_0/kg·kg^{-1}	2.454	0.889
E/kJ·kg^{-1}	287.26	222.4
n	0.945	0.898
average error of regression (%)	3.8	11.6

derived from the DA model with the adsorbed phase volume correction, and the broken lines show the isotherms without considering the adsorbed phase volume correction. The adsorption parameters (W_0/C_0, E, and n) are listed in Table 4. The average error of analysis is more than 11 % of the experimental data for the DA model in the case of no adsorbed phase volume consideration. However, the regression value agrees to within 4 % of experimental uptake values with the adsorbed phase volume correction. It proves that the adsorbed phase volume correction for the DA model, which was proposed by Ozawa et al.[29] for a wide range of temperatures with adsorbed phase thermal expansion consideration, is more appropriate for the present study.

In Figure 6, the differences between the experimentally measured and the calculated uptake ($C_{experiment} - C_{model}$) values are plotted against the experimental uptake ($C_{experiment}$). It can be seen that the DA model with adsorbed phase volume correction has the smallest ($C_{experiment} - C_{model}$) values. Thus, the DA model appears to be suitable for the theoretical analysis of the adsorbed methane storage system, as this model allows the accountability of the adsorbed phase volume correction for a wide range of pressures and temperatures.

Isosteric Heat of Adsorption. Figure 7 shows the uptake and temperature-dependent heat of adsorption (H_{ads}) at different isosteric conditions for the Maxsorb III/methane pair. The values of the heat of adsorption (H_{ads}) have been extracted from the isotherm data using the Clausius−Clayperon equation along with the correction term for the nonideality of the gaseous phase, recently derived by Chakrabarty et al.,[33] which is as follows.

$$H_{ads} = RT^2\left[\left(\frac{\partial(\ln P)}{\partial T}\right)_C\right] + Tv_g\frac{dP}{dT}(P,T) \tag{9}$$

Here, the first term of the right-hand side is derived from the Clausius−Clayperon equation and can be expanded by using

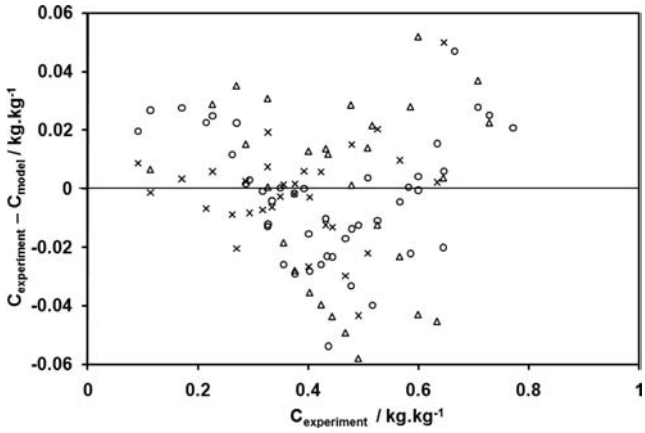

Figure 6. Comparison of the differences between the experimental and the calculated uptakes from the models: ○, Tóth model; ×, DA model with the adsorbed phase volume correction; △, DA model without considering the adsorbed phase volume.

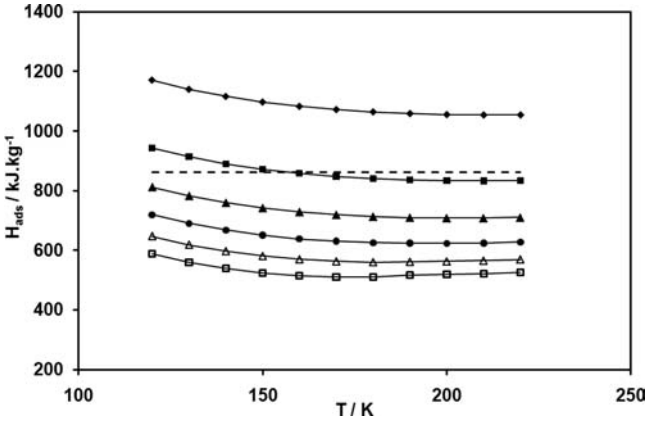

Figure 7. The heat of adsorption at different isosteric conditions calculated using eq 10: ♦, $C/C_0 = 0.1$ kg·kg^{-1}; ■, $C/C_0 = 0.2$ kg·kg^{-1}; ▲, $C/C_0 = 0.3$ kg·kg^{-1}; ●, $C/C_0 = 0.4$ kg·kg^{-1}; △, $C/C_0 = 0.5$ kg·kg^{-1}; □, $C/C_0 = 0.6$ kg·kg^{-1}. The horizontal broken line is from the Tóth model.

the DA isotherm model with adsorbed phase volume correction. The second term defines the behavior of the adsorbed mass with respect to changes in both the pressure and the temperature during adsorbate uptake, and this occurs due to the nonideality of the gaseous phase. Ultimately, eq 9 becomes

$$H_{ads} = 2RT + E\left[\left(\ln\frac{W_0}{Cv_a}\right)^{1/n} + \frac{1}{n}\left(\ln\frac{W_0}{Cv_a}\right)^{(1-n)/n}\right] + Tv_g\frac{dP}{dT}(P,T) \quad (10)$$

where v_g is the specific volume of the vapor phase and dP/dT represents the gradient of the pressure with the temperature of the adsorbate.

It can be seen that the heat of adsorption (H_{ads}) is high for low uptake and also varies with the temperature along the isosters (constant specific adsorbed amount). Therefore, the evolution of heat due to adsorption is higher during initial charge of gas in the ANG vessel which necessitates a very slow charge of gas for the initial period of charge cycle. In Figure 7, the horizontal broken line shows the average of H_{ads} over the whole range of concentration and temperature, and this value is derived from the Tóth isotherm model.

Henry's Law Coefficient. The Henry's law constant has been used as a criterion for the affinity of adsorption at low surface coverage. As the Tóth isotherm model is valid at both low and high pressure, it does possess the correct Henry law type behavior and the finite saturation limit.[28] So, the temperature-dependent Henry's law coefficients (K_H) at zero loading can be determined using the following equation.

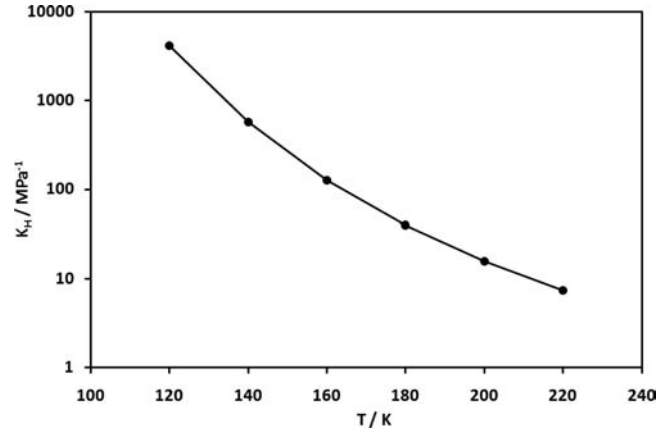

Figure 8. Henry's law coefficients at different temperatures.

$$K_H = \frac{\partial\theta}{\partial P}_{P\to 0} = k_0 \exp\left(\frac{\Delta h_{st}}{RT}\right) \quad (11)$$

where θ is the surface coverage for a certain temperature and is defined by C/C_0.

The coefficients for the methane/Maxsorb III pair at different temperatures are plotted in Figure 8. The K_H values decrease as the temperatures increase, which indicates the amount of gas adsorbed or desorbed is lesser at higher temperature, but the isosteric heat is the largest in the Henry's region.

Conclusion

A general purpose volumetric apparatus has been successfully incorporated with a cryostat where the uptake of pure methane on activated carbon type Maxsorb III has been measured for cryogenic temperatures ranging from (120 to 220) K and pressure up to 1.4 MPa. The experimental results have been regressed with different isotherm models and found to be well-described by the Tóth (regression error of 6 %) and the DA models (regression error of 4 %). However, the DA model has to perform a correction for the adsorbed phase volume. These isotherm results provide the necessary information about the charging pressure and temperature for ANG storage systems at the respective uptake capacity, especially when the NG is charged from the LNG terminal at near cryogenic temperatures. The calculated heat of adsorption is useful to predict the final temperature of the storage chamber after charging and also to analyze the other thermal properties such as internal energy, enthalpy, and entropy, and so forth.

Literature Cited

(1) Quinn, D. F.; Macdonald, J. A. Natural Gas Storage. *Carbon* **1992**, *30* (7), 1097–1103.
(2) Wegrzyn, J.; Gurevich, M. Adsorbent Storage of Natural Gas. *Appl. Energy* **1996**, *55* (2), 77–83.
(3) Talu, O. In *An Overview of Adsorptive Storage of Natural Gas*, Proceedings of the 4th International Conference On Fundamentals of Adsorption, Kyoto, Japan, International Adsorption Society, 1992; pp 655−662.
(4) Mota, J. P. B. Adsorbed natural gas technology. *Recent advances in adsorption processes for environmental protection and security*; Springer: Amsterdam, the Netherlands, 2008; pp 177−192.

(5) Bhatia, S. K.; Myers, A. L. Optimum Conditions for Adsorptive Storage. *Langmuir* **2006**, *22*, 1688–1700.
(6) Vasiliev, L. L.; Kanonchik, L. E.; Mishkinis, D. A.; Rabetsky, M. I. Adsorbed natural gas storage and transportation vessels. *Int. J. Therm. Sci.* **2000**, *39*, 1047–1055.
(7) Sun, Y.; Liu, C.; Su, W.; Zhou, Y.; Zhou, L. Principles of methane adsorption and natural gas storage. *Adsorption* **2009**, *15*, 133–137.
(8) Pupier, O.; Goetz, V.; Fiscal, R. Effect of cycling operations on an adsorbed natural gas storage. *Chem. Eng. Process.* **2005**, *44*, 71–79.
(9) Yang, X. D.; Zheng, Q. R.; Gu, A. Z.; Lu, X. S. Experimental studies of the performance of adsorbed natural gas storage system during discharge. *Appl. Therm. Eng.* **2005**, *25*, 591–601.
(10) Basumatary, R.; Dutta, P.; Prasad, M.; Srinivasan, K. Thermal modeling of activated carbon based adsorptive natural gas storage system. *Carbon* **2005**, *43*, 541–549.
(11) Lozano-Castelló, D.; Cazorla-Amorós, D.; Linares-Solano, A. Powdered Activated Carbons and Activated Carbon Fibers for Methane Storage: A Comparative Study. *Energy Fuels* **2002**, *16*, 1321–1328.
(12) Chen, X. S.; Mcenaney, B.; Mays, T. J.; Alcãniz, J.; Cazorla, D.; Linares-Solano, A. Theoretical and experimental studies of methane adsorption on microporous carbons. *Carbon* **1997**, *35* (9), 1251–1258.
(13) Saha, B. B.; Koyama, S.; El-Sharkawy, I. I.; Habib, K.; Srinivasan, K.; Dutta, P. Evaluation of Adsorption Parameters and Heats of Adsorption through Desorption Measurements. *J. Chem. Eng. Data* **2007**, *52*, 2419–2424.
(14) Celzard, A.; Albiniak, A.; Jasienko-Halat, M.; Marêché, J. F.; Furdin, G. Methane storage capacities and pore textures of active carbons undergoing mechanical densification. *Carbon* **2005**, *43*, 1990–1999.
(15) Himeno, S.; Komatsu, T.; Fujita, S. High pressure adsorption equilibria of methane and carbon dioxide on several activated carbons. *J. Chem. Eng. Data* **2005**, *50*, 369–376.
(16) Esteves, I. A. A. C.; Lopes, M. S. S.; Nunes, P. M. C.; Mota, J. P. B. Adsorption of natural gas and biogas components on activated carbon. *Sep. Purif. Technol.* **2008**, *62*, 281–296.
(17) Alcãz-monge, J.; Lozano-Castelló, D.; Cazorla-amórs, D.; Linares-solano, A. Fundamentals of methane adsorption in microporous carbons. *Microporous Mesoporous Mater.* **2009**, *124* (1−3), 110–116.
(18) Mota, J. P. B.; Rodrigljes, A. E.; Saatdjian, E.; Tondeur, D. Dynamics of natural gas adsorption storage systems employing activated carbon. *Carbon* **1997**, *35* (9), 1259–1270.
(19) Menon, V. C.; Komarneni, S. Porous Adsorbents for Vehicular Natural Gas Storage: A Review. *J. Porous Mater.* **1998**, *5*, 43–58.
(20) Macdonald, J. A.; Quinn, D. F. Carbon adsorbents for natural gas storage. *Fuel* **1998**, *77* (112), 61–64.
(21) Sircar, S.; Golden, T. C.; Rao, M. B. Activated carbon for gas separation and storage. *Carbon* **1996**, *34* (1), l–12.
(22) Matranga, K. R.; Myers, A. L.; Glandt, E. D. Storage of natural gas by adsorption on activated carbon. *Chem. Eng. Sci.* **1992**, *47* (7), 1569–1579.
(23) Lozano, D.; De la Casa, M. A.; Alcãniz, J.; Cazorla, D.; Linares, A. Advances in the study of methane storage in porous carbonaceous materials. *Fuel* **2002**, *81*, 1777–1803.
(24) Biloe, S.; Goetza, V.; Guillot, A. Optimal design of an activated carbon for an adsorbed natural gas storage system. *Carbon* **2002**, *40*, 1295–1308.
(25) Chakraborty, A.; Saha, B. B.; Ng, K. C.; Koyama, S.; Srinivasan, K. Theoretical Insight of Physical Adsorption for a Single-Component Adsorbent + Adsorbate System: II. The Henry Region. *Langmuir* **2009**, *25* (13), 7359–7367.
(26) Otowa, T.; Tanibata, T.; Itoh, M. Production and adsorption characteristics of MAXSORB: high-surface-area active carbon. *Gas Sep. Purif.* **1993**, *7* (4), 241–245.
(27) Setzmann, U.; Wagner, W. A new equation of state and tables of thermodynamic properties for methane covering the range from the melting line to 625 K at pressures up to 1000 MPa. *J. Phys. Chem. Ref. Data* **1991**, *20* (6), 1061–1151.
(28) Do, D. D. *Adsorption Analysis: Equilibria and Kinetics*; Imperial College Press: London, 1998.
(29) Ozawa, S.; Kusumi, S.; Ogino, Y. Physical Adsorption of Gases at High Pressure. *J. Colloid Interface Sci.* **1976**, *56*, 83–91.
(30) Dubinin, M. M. The potential theory of adsorption of gases and vapors for adsorbents with energetically nonuniform surfaces. *Chem. Rev.* **1960**, *60*, 1–70.
(31) Amankwah, K. A. G.; Schwarz, J. A. A modified approach for estimating pseudo vapor pressures in the application of the Dubinin−Astakhov equation. *Carbon* **1995**, *33*, 1313–1319.
(32) Loh, W. S.; Rahman, K. A.; Chakraborty, A.; Saha, B. B.; Choo, Y. S.; Khoo, B. C.; Ng, K. C. Improved Isotherm Data for Adsorption of Methane on Activated Carbons. *J. Chem. Eng. Data* **2010**, *55*, 2840–2847.
(33) Chakraborty, A.; Saha, B. B.; Koyama, S.; Ng, K. C. On the thermodynamic modeling of the isosteric heat of adsorption and comparison with experiments. *Appl. Phys. Lett.* **2006**, *89*, 171901.

Received for review May 21, 2010. Accepted September 3, 2010. The authors wish to express their gratitude for financial support from (i) the WCU program No. R-33-2009-000-10101660 of Korea, (ii) the AStar Grant No. R265-000-268-305/490, and (iii) the KAUST Grant R265-000-286-597.

JE1005328